

IrRep: symmetry eigenvalues and irreducible representations of *ab initio* band structures

Mikel Iraola^{a,b,*}, Juan L. Mañes^b, Barry Bradlyn^c, Titus Neupert^d, Maia G. Vergniory^{a,e,**},
Stepan S. Tsirkin^d

^a*Donostia International Physics Center, 20018 Donostia-San Sebastian, Spain*

^b*Department of Condensed Matter Physics, University of the Basque Country UPV/EHU, Apartado 644,
48080 Bilbao, Spain*

^c*Department of Physics and Institute of Condensed Matter Theory, University of Illinois at
Urbana-Champaign, IL 61801, USA*

^d*Department of Physics, University of Zurich, Winterthurerstrasse 190, CH-8057 Zurich, Switzerland*

^e*IKERBASQUE, Basque Foundation for Science, Maria Diaz de Haro 3, 48013 Bilbao, Spain*

Abstract

We present **IrRep** – a Python code that calculates the symmetry eigenvalues of electronic Bloch states in crystalline solids and the irreducible representations under which they transform. As input it receives bandstructures computed with state-of-the-art Density Functional Theory codes such as VASP, Quantum Espresso, or Abinit, as well as any other code that has an interface to Wannier90. Our code is applicable to materials in any of the 230 space groups and double groups preserving time-reversal symmetry with or without spin-orbit coupling included, for primitive or conventional unit cells. This makes **IrRep** a powerful tool to systematically analyze the connectivity and topological classification of bands, as well as to detect insulators with non-trivial topology, following the Topological Quantum Chemistry formalism: **IrRep** can generate the input files needed to calculate the (physical) elementary band representations and the symmetry-based indicators using the *CheckTopologicalMat* routine of the Bilbao Crystallographic Server. It is also particularly suitable for interfaces with other plane-waves based codes, due to its flexible structure.

Keywords: DFT; Symmetry; Irreducible representations; Topology; Python; Bandstructure.

PROGRAM SUMMARY

Program Title: IrRep

Developer's repository link: <https://github.com/stepan-tsirkin/irrep>

Licensing provisions: GPLv3

Programming language: Python

Nature of problem: Symmetry properties of electronic band structures in solids are tightly related

*E-mail: mikel.i.iraola@gmail.com

**E-mail: maiagvergniory@dipc.org

to their topological features. This relation is set mathematically by the formalisms of Topological Quantum Chemistry [1,2] and symmetry-based indicators of topology [3], but their application requires knowledge of the irreducible representations of the bands. Therefore, a code to calculate irreducible representations of *ab initio* bands is essential for a systematic theoretical search and classification of topological materials.

Solution method: **IrRep** reads wave functions from files generated by VASP, Abinit, or Quantum Espresso (also files written as input for Wannier90), determines the space group and symmetry operations via the **spglib** library, evaluates the eigenvalues of the symmetry operations for the selected bands, and applies Group Theory to determine their irreducible representations.

Additional comments: In Abinit calculations, **istwfk=1** should be used. Routines to get Wannier charge centers and Zak phase are also included, although they work reliably only with norm-conserving pseudopotentials.

References

- [1] Barry Bradlyn, L. Elcoro, Jennifer Cano, M. G. Vergniory, Zhijun Wang, C. Felser, M. I. Aroyo, and B. Andrei Bernevig, *Nature* 547, 298-305 (2017).
- [2] M. G. Vergniory, L. Elcoro, C. Felser, N. Regnault, B. A. Bernevig, and Z. Wang, *Nature* 566, A complete catalogue of high-quality topological materials, *Nature* 566, 480-485 (2019).
- [3] Hoi Chun Po, Ashvin Vishwanath, and Haruki Watanabe, *Nature Communications* 8, 50 (2017).

1. Introduction

Symmetries are fundamental to the properties of quantum systems[1]. In particular, knowledge of the symmetry operations under which energy eigenstates transform is crucial to determine the degeneracy of energy levels, the allowed couplings to external fields, and the effect of symmetry-breaking perturbations. For instance, the degeneracies present in the vibrational spectrum of a molecule are determined by the dimensions of its symmetry group’s irreducible (co-)representations (IRs). For electrons in periodic crystals, the band structure of a material in reciprocal space cannot be characterized without studying the symmetry properties of its wave functions[2, 3]: symmetries can protect or prevent band crossings, predict splittings produced by spin-orbit coupling, and explain gap openings coming from specific terms in the Hamiltonian.

With the discovery of topological insulators[4, 5], the symmetry analysis of band structures has regained importance. Recently it was discovered that electrons in periodic lattices with crystalline symmetries can yield rich physics due to the interplay of symmetry and topology[6–12]. Two main developments in the application of symmetry to the identification and classification of topological insulators gave a gigantic push to the field: First, the theory of Topological Quantum Chemistry (TQC)[13–15] built upon physical elementary band representations (PEBRs) classified all possible atomic limits in all nonmagnetic materials,

identifying topological bands as those that cannot be expressed as a sum of band representations. Among the topological bands, a subset can be distinguished from trivial bands by computing a set of symmetry-based indicators[16–18] from the irreducible representations under which the bands transform. The set of symmetry-based indicators in each space group can be computed from the band representations, and have been tabulated in [19, 20]. Calculation of the IRs of bands at high symmetry points is fundamental for the application of these methods and has lead to the prediction of many topological insulators[21–24] and new phases[25–35].

In this work we present **IrRep**, a robust, open source Python code that calculates symmetry eigenvalues and IRs of the wave-functions at high symmetry points in reciprocal space for any band structure computed by means of Density Functional Theory (DFT). Currently, **IrRep** can interface directly with 3 widely used plane-wave DFT codes: the Vienna Ab initio Simulation Package (VASP)[36], Abinit[37] and Quantum Espresso (QE)[38]. **IrRep** can also read input files in Wannier90 (W90)[39] format (`.win`, `.eig`, `_UNK`), prepared by interfaces like `pw2wannier90`. This allows **IrRep** to be used with any code that has a W90 interface, such as SIESTA[40]. Furthermore, **IrRep** has been structured in a user friendly format allowing the implementation of routines to interface with any other plane-wave based code.

Although similar codes exist for VASP[41] (*vasp2trace*, used to calculate the topological bands in [21, 42, 24] materials database) and QE[43], **IrRep** is the only code that does not restrict the user to a single DFT program. Moreover, our code follows the same notation as the popular Bilbao Crystallographic Server (BCS)[44] to identify the IRs, which avoids confusion coming from the lack of an official standard notation, especially for spin-orbit coupled systems. Tables of IRs are encapsulated within the code package, so that **IrRep** can determine IRs without extra input from the user. The output is written in a form that is compatible with the *CheckTopologicalMat* tool of the BCS[21]. As additional functionality, **IrRep** can separate bands by eigenvalues of certain symmetry operator and calculates the \mathbb{Z}_2 and \mathbb{Z}_4 topological indices of time-reversal symmetric band structures[4]. The code evolved from the routines written for Ref. [45] to determine the eigenvalues of screw rotations. At a testing level, the code was used in Refs. [28, 46–49] for topological quantum chemistry analysis, and in Refs. [50, 51] to analyze the dipole selection rules for optical matrix elements. According to Ref. [52] it has been downloaded more than 7000 times. In section 2 we will introduce the basic concepts of group theory underlying the operation of **IrRep**. In section 3 we will present the workflow of the code. Finally, section 4 will be devoted to several examples, illustrating the capabilities of **IrRep** code for the analysis of symmetry and topology.

2. Symmetry Properties of Bands: Irreducible Representations

In this section we give a brief overview of the application of group theory to electronic Bloch states. However, only the minimal information necessary to introduce the notation and explain the functionality of the code is provided. More details may be found in classic textbooks such as [3, 53].

The group G of symmetry operations that leaves a crystal invariant is called the space group of the crystal. In particular, G contains all translations by vectors of the Bravais

lattice. The (infinite) group of all translations is generated by 3 primitive basis vectors of the lattice, and forms the (normal) translation subgroup T of the space group G . This allows us to write the coset decomposition of G with respect to T ,

$$G = T + g_1 T + g_2 T + \dots + g_N T, \quad (1)$$

where g_1, g_2, \dots, g_N are called the coset representatives of the decomposition. Notice that the set of coset representatives is finite and non-unique (two coset representatives differing by a translation characterize the same coset). The number N of cosets in the decomposition Eq. (1) is equal to the order of the point group $\bar{G} = G/T$ (though the set of coset representatives themselves need not be a point group for non-symmorphic lattices). Using this decomposition, any space group can be expressed in terms of the coset representatives and lattice vectors of the Bravais lattice.

The symmetries of the space group have a well-defined action on the Hilbert space of electronic states in the crystal. We denote by U_g the representation of a certain symmetry operation $g \in G$ on the Hilbert space. Since every $g \in G$ is a symmetry of the crystal, each representation matrix U_g commutes with the Hamiltonian matrix H , i.e., $[U_g, H] = 0$. Note that H is block diagonal in reciprocal space and each block $H(\mathbf{k})$ can be put in correspondence to a vector \mathbf{k} belonging to the first Brillouin zone (BZ). Although the whole matrix H commutes with U_g , for a general $g \in G$, a block $H(\mathbf{k})$ may not commute, but rather must be linearly related to $H(g\mathbf{k})$, i.e. the operation g transforms \mathbf{k} into another reciprocal vector $g\mathbf{k}$. If we use Wigner-Seitz notation $g = \{R|\mathbf{v}\}$ for the space group operations, then $g\mathbf{k} = R\mathbf{k}$. The set of $g \in G$ that leaves \mathbf{k} invariant (up to a reciprocal lattice vector \mathbf{G}) is called the little group $G_{\mathbf{k}}$ of \mathbf{k} .

Note that the coset decomposition of Eq. (1) can also be applied to the little group $G_{\mathbf{k}}$:

$$G_{\mathbf{k}} = T + g_1^{\mathbf{k}} T + g_2^{\mathbf{k}} T + \dots + g_M^{\mathbf{k}} T, \quad (2)$$

where $M \leq N$ since $G_{\mathbf{k}} < G$. The coset representatives $g_i^{\mathbf{k}}$ can all be chosen to be point group elements only if $G_{\mathbf{k}}$ is a symmorphic space group. For example, a group containing screw rotations or glide reflections does not contain its point group as a subgroup. In any case, the rotational parts R_i of the representatives $g_i^{\mathbf{k}} = \{R_i|\mathbf{v}_i\}$ do form a point group $\bar{G}_{\mathbf{k}}$, called little co-group of \mathbf{k} . While the little group $G_{\mathbf{k}}$ is infinite, since it contains all translations, the little co-group $\bar{G}_{\mathbf{k}}$ is finite.

Consider a set $\{|\Psi_{1\mathbf{k}}\rangle, |\Psi_{2\mathbf{k}}\rangle, \dots, |\Psi_{D\mathbf{k}}\rangle\}$ of eigenstates of $H(\mathbf{k})$, closed under the action of $G_{\mathbf{k}}$. When a symmetry operation $g \in G_{\mathbf{k}}$ acts on $|\Psi_{n\mathbf{k}}\rangle$, the state undergoes a linear transformation

$$g|\Psi_{i\mathbf{k}}\rangle = \sum_{j=1}^D K^{ji}(g) |\Psi_{j\mathbf{k}}\rangle. \quad (3)$$

The matrices $K(g)$ in Eq. (3) form the representation K of $G_{\mathbf{k}}$ defined in the invariant space spanned by $\{|\Psi_{n\mathbf{k}}\rangle\}_D$. It is said that K is an IR, if this space cannot be divided into smaller

non-trivial invariant subspaces. Every representation is characterized by the set of traces $\chi_K(g) = \text{Tr}K(g)$, known as the *character* of the representation.

In general, the closed set $\{|\Psi_{n\mathbf{k}}\rangle\}_D$ contains eigenstates transforming under more than one IR of $G_{\mathbf{k}}$, meaning that the whole representation K is reducible and can be decomposed as a combination of these IRs

$$K = \oplus_{\alpha} m_{\alpha}^{\mathbf{k}} K_{\alpha}, \quad (4)$$

where K_{α} is the α^{th} IR of $G_{\mathbf{k}}$. Its multiplicity $m_{\alpha}^{\mathbf{k}}$ can be computed by means of the following expression, often referred to as the *magic formula* [54, 55]

$$m_{\alpha}^{\mathbf{k}} = \frac{1}{||\bar{G}_{\mathbf{k}}||} \sum_{g \in \{g_i^{\mathbf{k}}\}} \chi_K^*(g) \chi_{\alpha}(g), \quad (5)$$

with $\{g_i^{\mathbf{k}}\}$ denoting the set of coset representatives in the decomposition of $G_{\mathbf{k}}$, and $||\bar{G}_{\mathbf{k}}||$ the number of symmetry operations in the little cogroup $\bar{G}_{\mathbf{k}} = G_{\mathbf{k}}/T$. χ_{α} and χ_K indicate the characters corresponding to the IR K_{α} and the representation K to be decomposed, respectively. **IrRep** uses this formula to determine the IRs of the eigenstates of $H(\mathbf{k})$ at high-symmetry points in the BZ.

3. Implementation in IrRep code

In this section, we present the workflow of the **IrRep** code and describe its main functionalities and the particularities of the interface to each DFT software.

3.1. Reading DFT data and input parameters

To keep the interaction with the user simple, **IrRep** reads as much needed information as possible from the DFT codes output files. Only parameters determining the user-defined task should be given in the command line in the format

```
1 python -m irrep <keyword1>=<value1> <keyword2>=<value2> ...
```

Among all options, the most important ones can be found in Tab. 1. Depending on the DFT code used to calculate wave functions, a different interface should be chosen. The interfaces are selected with the keyword `code`; currently, it includes interfaces to VASP [36], Abinit [37] and QE [38]. It can also read the input files for W90 [39], which allows **IrRep** to be used with any of the multiple codes that support the Wannier90 interface. Note that no user-defined input file is needed, and the rest of the needed information will be read from the DFT output files (see Table 2). While most of the keywords are self-explanatory, the meaning of the keywords `refUC` and `shiftUC` requires some elaboration. The tables of IRs are written for the conventional unit cell corresponding to the space group, i.e. the cell whose lattice vectors are parallel to the symmetry directions of the lattice. However, the DFT calculation may be done in any unit cell. Let $\{\mathbf{a}_1, \mathbf{a}_2, \mathbf{a}_3\}$ denote the basis vectors of the cell adopted for the calculation and $\{\mathbf{c}_1, \mathbf{c}_2, \mathbf{c}_3\}$ those of the conventional setting, `refUC` is the 3×3 matrix M that expresses the relation between them, according to the following expression

$$(\mathbf{c}_1, \mathbf{c}_2, \mathbf{c}_3)^T = M(\mathbf{a}_1, \mathbf{a}_2, \mathbf{a}_3)^T \quad (6)$$

Keyword	Function
fWAV	VASP input file with wave functions. Default: WAVECAR
fPOS	VASP input file with the crystal structure. Default: POSCAR
fWFK	Abinit input file with wave functions
prefix	variable prefix in QE calculation or seedname in W90
IBstart	first band to be considered
IBend	last band to be considered
code	name of the DFT code: vasp , espresso , abinit , wannier90
spinor	whether wave functions are spinors or not (T/F, only needed for VASP)
Ecut	plane wave cutoff to be applied (in eV), recommended ≈ 50 eV
kpoints	indices of k -points at which IRs must be computed
kpnames	labels of k -points at which IRs must be computed
refUC	transformation of basis vectors with respect to standard setting
shiftUC	shift of origin with respect to standard setting
onlysym	stop after finding symmetries
ZAK	calculate Zak phases
WCC	calculate wannier charge centers

Table 1: Principal keywords to fix running options with **IrRep** and their function.

Similarly, **shiftUC** describes the shift of the origin with respect to the origin of the conventional unit cell. Note that **shiftUC** and **refUC** are relevant only to determine the names of IRs in the notation of BCS. The characters can be computed with any choice of unit cell.

In order to illustrate the use of these keywords, we work out the example of the C-centered monoclinic structure. Let the relation between the conventional basis vectors and the primitive ones used in the DFT calculation be the following, as illustrated in Fig. 1

$$\begin{aligned}
\mathbf{c}_1 &= \mathbf{a}_1 + \mathbf{a}_2, \\
\mathbf{c}_2 &= -\mathbf{a}_1 + \mathbf{a}_2, \\
\mathbf{c}_3 &= \mathbf{a}_3.
\end{aligned}$$

Also, assume that the two origins are related by the shift $0.3\mathbf{a}_3$. Then, the keywords **refUC** and **shiftUC** should be used with arguments

```
1 refUC=1,1,0,-1,1,0,0,0,1 shiftUC=0,0,0.3
```

interface	code=	files
VASP	vasp	POSCAR and WAVECAR
Abinit	abinit	*.WFK
QE	espresso	*.save/data_file_schema.xml and *.save/wfc*.dat
Wannier90	wannier90	*.win, *.eig, UNK*

Table 2: Files read by **IrRep** depending on the chosen interface

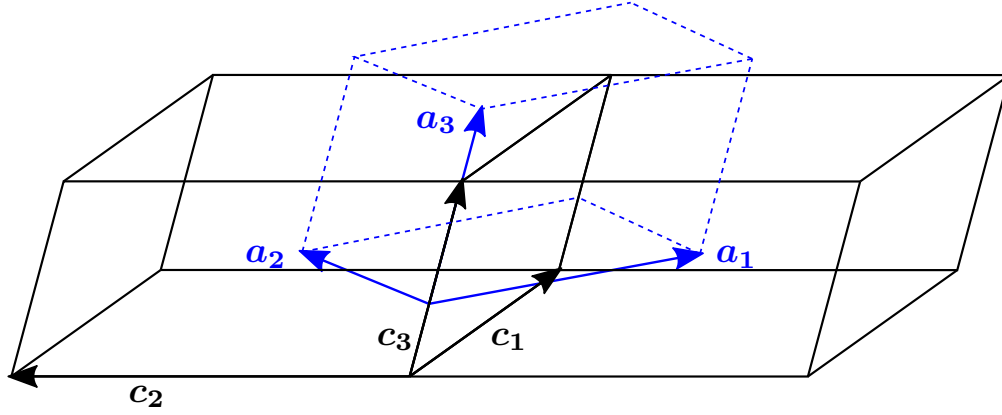


Figure 1: The two choices considered for the unit cell of the C-centered monoclinic structure. Conventional (primitive) basis vectors are indicated in black (blue). The conventional unit cell is marked by solid black lines, while the primitive cell is dashed blue.

When a basis transformation is applied, symmetry operations will be printed in both basis. For instance, the following lines illustrate the operations (only identity and inversion) printed by the code in the example of the C-centered crystal:

```

1 Space group # 12 has 4 symmetry operations
2 # 1
3 rotation : | 1  0  0 |      in refUC : | 1  0  0 |
4           | 0  1  0 |           | 0  1  0 |
5           | 0  0  1 |           | 0  0  1 |
6 translation : [ 0.000000  0.000000  0.000000 ]
7   in the reference unit cell :
8   translation : [ 0.000000  0.000000  0.000000 ]
9 axis: [0. 0. 1.] ; angle = 0 , inversion : False
10 # 2
11 rotation : | -1  0  0 |      in refUC : | -1  0  0 |
12           | 0 -1  0 |           | 0 -1  0 |
13           | 0  0 -1 |           | 0  0 -1 |
14 translation : [ 0.000000  0.000000  0.400000 ]
15   in the reference unit cell :
16   translation : [ 0.000000  0.000000  0.000000 ]

```

Once keywords are provided, the class `BandStructure` reads the basic information from the output files of the DFT code, such as the plane-wave cutoff, Fermi energy, number of bands, etc. In essence, the lattice vectors, positions of atoms and the energies and wavefunctions of electronic states are read in this way (see Sec. 3.3 for details). These parameters are found in the files listed in Table 2.

When the information is read, it is stored in an object of class `Bandstructure` which is independent of the ab initio code used. Thus, if an interface to a new ab initio code is needed, one has to simply implement another constructor for the `Bandstructure` class.

3.2. Determination of the space group

Next, basis vectors and atomic positions are passed to the library Spglib [56], whose routine `get_spacegroup` gives the name and number of the space group, while `get_symmetry` returns the coset representatives of the space group's decomposition with respect to the translation group (see Sec. 2 for details). At this point, if the flag `onlysym` in Tab. 1 was set, `IrRep` prints the crystal structure and aforementioned coset representatives and then stops. Note that this utility can be useful for VASP even before running the DFT calculation to make sure that the configuration described in POSCAR really matches the assumed space group.

3.3. Reading wave functions

In VASP, Abinit and QE, eigenstates $|\Psi_{n\mathbf{k}}\rangle$ of $H(\mathbf{k})$ are expanded in a basis of plane waves $|\mathbf{k} + \mathbf{G}\rangle$:

$$|\Psi_{n\mathbf{k}}\rangle = \sum_{\mathbf{G}} C_{n\mathbf{k}}(\mathbf{G}) |\mathbf{k} + \mathbf{G}\rangle, \quad (7)$$

where the sum runs over all the reciprocal lattice vectors \mathbf{G} whose energy is smaller than a cutoff, i.e. $\hbar^2(\mathbf{k} + \mathbf{G})^2/2m_e < E_{\text{cut}}$. The cutoff coincides with the value indicated by the user if E_{cut} in Tab. 1 was set; otherwise, it will be the cutoff used in the DFT calculation. After testing the code with different systems, we have noticed that usually a value $E_{\text{cut}} \sim 50$ eV yields accurate results, since the most dominant coefficients in Eq. (7) correspond to short \mathbf{G} . After the application of the cutoff, the eigenstates $|\Psi_{n\mathbf{k}}\rangle$ are normalized.

If the DFT calculation ran with PAW pseudopotentials [57–59], the expansion Eq. (7) gives the smooth pseudo-wavefunctions $|\tilde{\Psi}_{n\mathbf{k}}\rangle$, which are related to the all-electron wavefunctions $|\Psi_{n\mathbf{k}}\rangle$ by a linear transformation $|\Psi_{n\mathbf{k}}\rangle = \mathcal{T}|\tilde{\Psi}_{n\mathbf{k}}\rangle$. Note that $|\tilde{\Psi}_{n\mathbf{k}}\rangle$ and $|\Psi_{n\mathbf{k}}\rangle$ transform under symmetry operations in the same way. Hence for simplicity we work with the pseudo-wavefunctions.

In the Wannier90 input files (UNK*) the wavefunctions are written on a real-space grid. In that case we perform a fast Fourier transform (FFT) to obtain the coefficients $C_{n\mathbf{k}}(\mathbf{G})$ of Eq. (7).

3.4. Calculation of traces

For each \mathbf{k} , symmetry operations g of its little group are picked one by one and expectation values $\langle\Psi_{n\mathbf{k}}|g|\Psi_{n\mathbf{k}}\rangle$ are calculated. Note that since the transformation properties of plane waves under translations are trivial, we need only iterate through the coset representatives $g_i^{\mathbf{k}}$. The calculation of the overlaps depends on whether the DFT calculations were performed on scalar or spinor wavefunctions. Let us consider a $g = \{R|\mathbf{v}\} \in G_{\mathbf{k}}$ and show the calculation in both cases:

- scalar wavefunctions:

$$\langle\Psi_{n\mathbf{k}}|g|\Psi_{n\mathbf{k}}\rangle = \sum_{\mathbf{G}\mathbf{G}'} C_{n\mathbf{k}}^*(\mathbf{G}') C_{n\mathbf{k}}(\mathbf{G}) \langle\mathbf{k} + \mathbf{G}'|\{R|\mathbf{v}\}|\mathbf{k} + \mathbf{G}\rangle. \quad (8)$$

From the transformation property of plane-waves,

$$g|\mathbf{k} + \mathbf{G}\rangle = e^{-i(R\mathbf{k} + R\mathbf{G}) \cdot \mathbf{v}} |R\mathbf{k} + R\mathbf{G}\rangle, \quad (9)$$

together with their orthogonality property,

$$\langle \mathbf{k}' + \mathbf{G}' | \mathbf{k} + \mathbf{G} \rangle = \delta_{\mathbf{G}', \mathbf{k} - \mathbf{k}' + \mathbf{G}}, \quad (10)$$

it follows that Eq. (8) is reduced to:

$$\langle \Psi_{n\mathbf{k}} | g | \Psi_{n\mathbf{k}} \rangle = \sum_{\mathbf{G}} C_{n\mathbf{k}}^*(R\mathbf{k} - \mathbf{k} + R\mathbf{G}) C_{n\mathbf{k}}(\mathbf{G}) e^{-i(R\mathbf{k} + R\mathbf{G}) \cdot \mathbf{v}}. \quad (11)$$

- for spinor wavefunctions $|\Psi_{n\mathbf{k}}\rangle = (|\Psi_{n\mathbf{k}}^\uparrow\rangle |\Psi_{n\mathbf{k}}^\downarrow\rangle)^T$ the matrix element reads:

$$\langle \Psi_{n\mathbf{k}} | g | \Psi_{n\mathbf{k}} \rangle = \sum_{\sigma\sigma'} S_{\sigma\sigma'}(g) \langle \Psi_{n\mathbf{k}}^\sigma | g | \Psi_{n\mathbf{k}}^{\sigma'} \rangle, \quad (12)$$

where brackets $\langle \Psi_{n\mathbf{k}}^\sigma | g | \Psi_{n\mathbf{k}}^{\sigma'} \rangle$ are computed by means of Eq. (11) and $S(g)$ is an SU(2) matrix corresponding to g .

After this calculation, **IrRep** adds the expectation values of degenerate eigenstates. Each of these sums is the trace $\chi(g)$ of a matrix $K(g)$ belonging to the representation K defined in the subspace of degenerate eigenstates. These traces might be of interest by themselves, but can also be further used to identify the IRs.

3.5. Identification of irreducible representations

The characters χ_α of every IR K_α of $G_{\mathbf{k}}$ were obtained from the BCS [54] and are provided with the **IrRep** module. For each subspace of degenerate eigenstates, the magic formula (5) is applied, yielding the multiplicity $m_\alpha^{\mathbf{k}}$ of IR K_α in the subspace of degenerate states. Notice that this procedure detects accidental degeneracies, which happen when eigenstates transforming under different IRs have the same energy.

At this point, the IR of each set of eigenstates is printed, together with the character of the IR. Furthermore, **IrRep** also writes a file **trace.txt**, which can be passed directly to the program *CheckTopologicalMat* of BCS [44], in order to get information about (physical) elementary band representations and symmetry-based indicators [13, 19–21] to diagnose the band topology.

By default, the procedure is performed for all the bands calculated by the DFT code. Nevertheless, the user can set values for **IBstart** and **IBend** in order to consider only bands in the range **[IBstart, IBend]**. This can be used to noticeably shorten the calculation time. Moreover, for the selected set of bands, the smallest direct and indirect gaps with respect to higher bands will be printed. For centrosymmetric crystals, the number of inversion-eigenvalue inversions (band inversions) and the \mathbb{Z}_2 index [6, 60] will also be printed. In Sec. 4.1, we show an example of the output generated by **IrRep** where all these features are represented.

3.6. Separation by symmetry eigenvalues

When writing the IRs, **IrRep** can separate the states by their eigenvalues with respect to a certain symmetry operation, if the index of that symmetry was given as `isymsep` (Tab. 1). Moreover, wave functions can be grouped by Kramers pairs, via the key `groupKramers`. The energies will also be written in a file, which can be used to plot bands. This data will be useful if the DFT calculation was done for an ordered set of k -points following a certain path in the BZ. Bands with different symmetry eigenvalues will be written in different files. The purpose of this feature is to respect the separation in the plot of bands, which is useful to study the role of symmetries in the protection of band crossings [45].

IrRep also contains routines to calculate the Zak phase and Wannier charge centers of a given set of bands (see keys `ZAK` and `WCC` in Tab. 1).

Note that these functionalities work stably only for calculations employing norm-conserving pseudopotentials, and `Ecut` should not be specified in the command line (thus the DFT cutoff will be used). With the PAW method, due to the lack of consideration of the all-electron wavefunction, the results for symmetry separation and ZAK phase may be unreliable.

4. Example materials

In this section, we present the application of **IrRep** to two material examples, with different symmetries and topology, and analyzed by different DFT codes. With these examples, we cover the main functionalities of the code and also the subtlety related to the transformation between primitive and conventional basis.

4.1. Irreducible representations in CuBi_2O_4

First, we show the application of **IrRep** to CuBi_2O_4 . In the paramagnetic phase, this material crystallizes in a tetragonal structure characterized by the non-symmorphic space group $P4/ncc$ (No. 130) [61, 62]. Its crystal structure and BZ are shown in Fig. 2.

An interesting aspect of CuBi_2O_4 is found in reciprocal space: the little group of point $A=(1/2, 1/2, 1/2)$, in the corner of the BZ, has only one (double-valued) IR with dimension 8. Its unusually large dimension makes it promising for the realization of high-degeneracy unconventional fermions [63, 64]. Also due to the fact that the number of electrons in the unit cell is not a multiple of 8, this IR forces CuBi_2O_4 to be a filling-enforced semimetal.

We have calculated the band structure of CuBi_2O_4 with Abinit, both treating spin trivially (scalar calculation) and including spin-orbit corrections (spinor calculation). A plane-wave cutoff of 500 eV and cold smearing [65] were used in the calculation. The BZ was sampled with a grid of $5 \times 5 \times 7$. Lattice parameters and atomic positions were taken from the Topological Quantum Chemistry database of materials [21]. The exchange-correlation term was approximated through General Gradient Approximation, in the Perdew Burke Ernzerhof [66] parametrization and PAW pseudopotentials were taken from Pseudo Dojo database [67]. Computed band structures can be seen in Fig. 3. Output files of **IrRep** are available in the **examples** folder of **IrRep**'s official Github repository [68].

In the rest of the analysis, we focus on the partially-filled isolated set of bands cut by the Fermi level. IRs of the wave functions at high-symmetry points can be calculated by running the following lines (case without SOC):

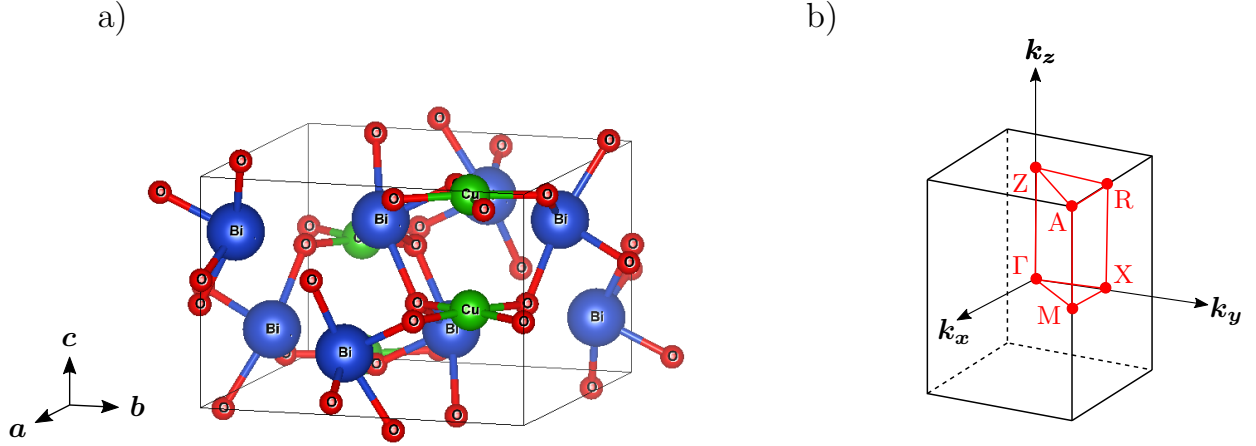


Figure 2: Crystal structure of CuBi_2O_4 . (a) Unit cell, with Cu, Bi and O atoms in green, blue and red, respectively. (b) BZ and irreducible BZ (red), with high-symmetry points.

```
1 python -m irrep code=abinit kpnames=GM,X,M,Z,R,A
2 Ecut=100 spinor=F fWFK=CuBi2O4-scalar_WFK
3 IBstart=145 IBend=148
```

IRs obtained in this way are written in Tab. 3. The following lines illustrate part of the output for the point $R = (0, 1/2, 1/2)$. Even though the little group of R contains many coset representatives, only two of them (represented by indices 1 and 7) are shown here for brevity.

Γ	X	M	Z	R	A
$\Gamma_4^+ \oplus \Gamma_2^+ \oplus \Gamma_4^- \oplus \Gamma_2^-$	$X_2 \oplus X_1$	$M_4 \oplus M_3$	$2Z_1$	$R_1 R_2$	$A_3 A_4$
$2\bar{\Gamma}_6 \oplus 2\bar{\Gamma}_8$	$2\bar{X}_3 \bar{X}_4$	$2\bar{M}_5$	$2\bar{Z}_5 \bar{Z}_7$	$\bar{R}_4 \bar{R}_4 \oplus \bar{R}_3 \bar{R}_3$	$\bar{A}_5 \bar{A}_5$

Table 3: IRs at high-symmetry points of the partially filled set of bands of CuBi_2O_4 . In the second (third) row, IRs of the calculation without (with) SOC included are listed.

```
1 k-point 5 :[0. 0.5 0.5]
2 number of irreps = 8
3 Energy | multiplicity | irreps | sym. operations
4 | | | | 1 7
5 -0.1006 | 4 | -R4(2.0) | 4.0+0.0j -4.0+0.0j
6 -0.0595 | 4 | -R3(2.0) | 4.0+0.0j 4.0+0.0j
7 inversion is # 9
8 number of inversions-odd Kramers pairs : 2
9 Gap with upper bands : 2.02
```

Interesting information about the bands and even about the chemistry of the system can be extracted from the knowledge of IRs. This set of IRs is consistent with an elementary band representation [13] induced from Wannier functions sitting in Wyckoff position $4c$: $(B \uparrow G)_{4c}$ in the case without SOC, $({}^1\bar{E}_2^2\bar{E}_2 \uparrow G)_{4c}$ with SOC, in the notation of Ref. [13]. According to the framework of band representations [69, 70], which explains how bands in reciprocal

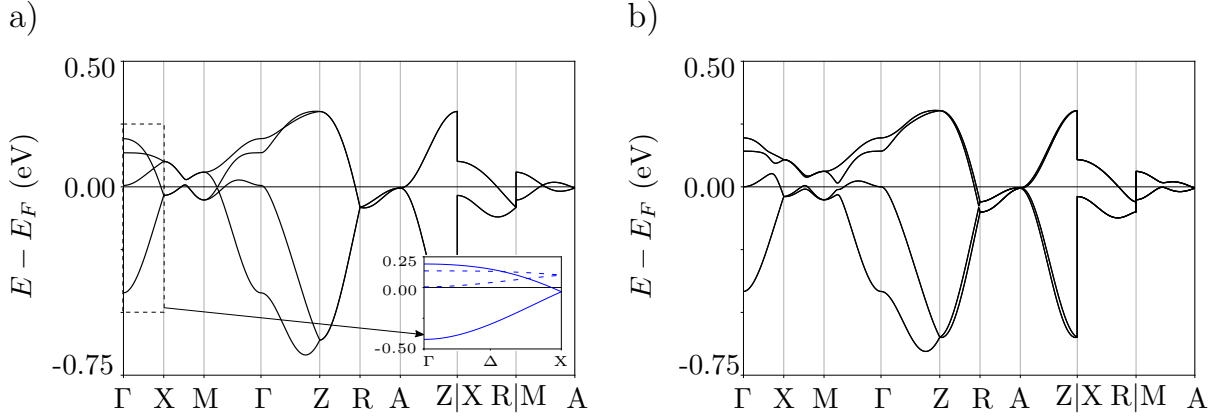


Figure 3: Band structure of CuBi_2O_4 (a) without SOC included. Inset: bands in line Δ , connecting Γ to X , separated according to their eigenvalue of symmetry $\{m_x|1/2, 0, 1/2\}$ in the little group: solid (dashed) corresponds to eigenvalue -1 ($+1$). (b) Band structure of CuBi_2O_4 with SOC included.

space inherit their symmetry properties from orbitals in real space, the Wannier functions that induce these bands transform as a combination of $d_{x^2-y^2}$ and d_{xy} orbitals.

At every point \mathbf{k} belonging to the line Δ that connects Γ to X , the little group contains the glide symmetry $g_x = \{m_x|1/2, 0, 1/2\}$. This means that for $\mathbf{k} \in \Delta$, wave functions of bands are also eigenstates of g_x , so that we can distinguish them by their eigenvalue under this symmetry. As we mentioned, **IrRep** can extract this eigenvalue, by running the option `isymsep=13`, which corresponds to g_x :

```
1 python -m irrep code=abinit Ecut=100 spinor=F
2   fWFK=CuBi2O4-scalar_WFK IBstart=145 IBend=148
3   isymsep=13
```

The index corresponding to g_x can be derived beforehand by running the option `onlysym`. The result is shown in the inset of Fig. 3(a), where bands with eigenvalue -1 ($+1$) of g_x are indicated in solid (dashed). This calculation tells us that the crossings between dashed and solid bands are protected by g_x and thus cannot be gapped out without breaking this symmetry. Such criteria can be used to systematically study symmetry protected band crossings [45].

4.2. Bismuth: high order topological insulator

In this example, we will present the calculation of \mathbb{Z}_2 and \mathbb{Z}_4 indices with **IrRep**. For that, we will work with a particularly interesting and well-known material: bismuth.

In the presence of only time-reversal symmetry (TRS), an insulator can belong to either the trivial or the topological phase. The system cannot undergo a transition from one phase to the other if the gap is not closed or TRS is not broken in the process. In this spirit, the topology of the system can be characterized by a \mathbb{Z}_2 invariant [4, 71, 60], which is -1 ($+1$) in the topological (trivial) phase. With inversion, the \mathbb{Z}_2 invariant can be calculated by multiplying the inversion eigenvalues of Kramers pairs of occupied bands at all time-

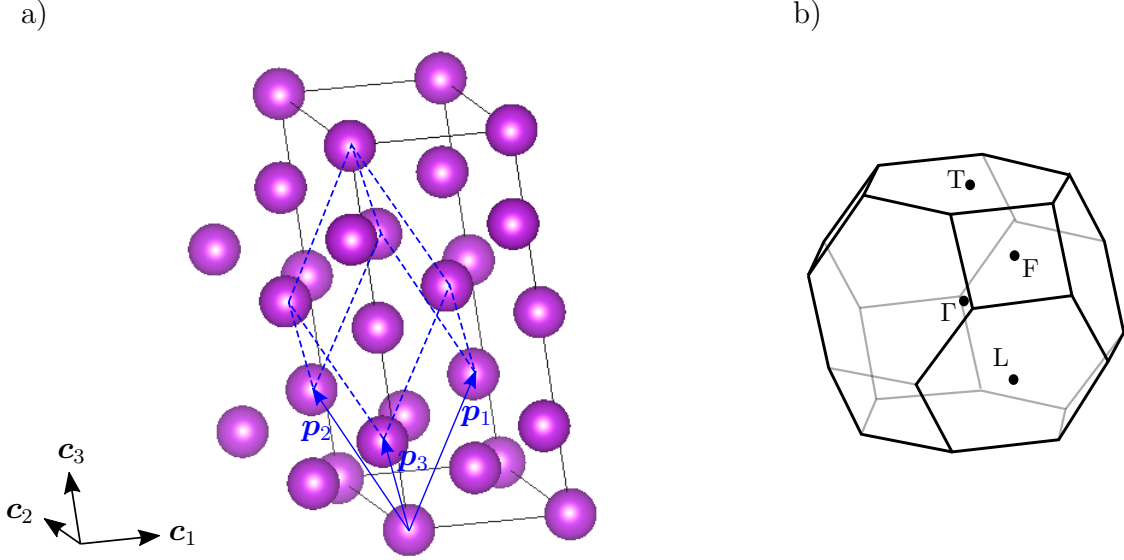


Figure 4: a) Crystal structure of Bi in space group $R\bar{3}m$. Black lines delimit the conventional unit cell, whose basis vectors are $\{c_i\}_{i=1,3}$, while blue lines delimit the primitive unit cell used in the DFT calculation. b) Brillouin Zone corresponding to the primitive cell and TRIM (one from each star of k -points).

reversal invariant momenta (TRIM)[6]. In the topological case, we say that the system has a band-inversion.

Crystal symmetries may enrich the topology of time-reversal invariant insulators, giving access to new phases, some of which can not be detected by the \mathbb{Z}_2 index. This is the case for bismuth in space group $R\bar{3}m$: the \mathbb{Z}_2 index has value +1, which means that the ground state corresponding to the occupied bands in Bi is a trivial insulator as per its \mathbb{Z}_2 index, according to the discussion above. However, in Ref. [27] it was shown that the ground state belongs to a higher-order topological phase, characterized by a \mathbb{Z}_4 index equal to 2. Here, we will reproduce with **IrRep** this analysis.

We have used VASP to perform *ab initio* calculations of Bi in the primitive unit cell. All calculations include spin-orbit corrections. A cutoff of 520 eV was set for the plane-wave basis, together with a Gaussian smearing. The BZ was sampled with a grid of $7 \times 7 \times 7$ k -points. We used PBE prescription as an approximation for the exchange-correlation term and PAW pseudopotentials [66]. The calculated bands are shown in Fig. 5(a). In Fig 5(b), we show the bands separated by eigenvalues of C_{3z} using **IrRep**'s option **isymsep**.

Space group $R\bar{3}m$ (No. 166) belongs to the rhombohedral family, in which conventional and primitive unit cells do not match, as can be seen in Fig. 4(a). Consequently, in order to use **IrRep** to get the IRs, we need to provide it with the transformation from the primitive to the conventional unit cell, via the keywords **refUC** and **shiftUC**. Since the origin of both, primitive and conventional cells is located in the same point, there is no need to specify

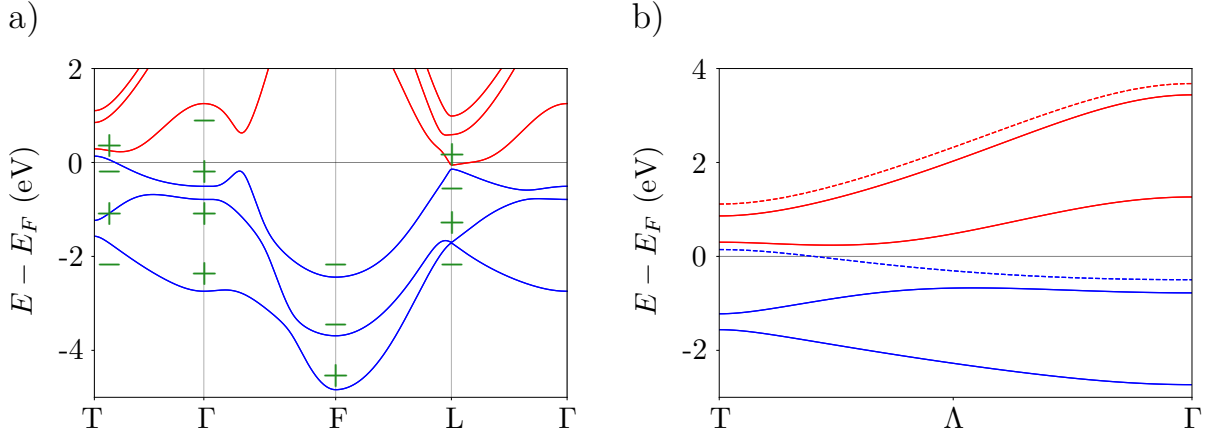


Figure 5: Band structure of Bi in space group $R\bar{3}m$. Since blue and red bands do not touch, we will ignore the electron-hole pockets and speak of occupied (blue) and unoccupied (red) bands. (a) Inversion eigenvalues at TRIM are indicated in green. (b) Bands along C_{3z} -invariant line Λ , which connects T to Γ ; solid and dashed bands have C_{3z} eigenvalues -1 and $\exp(\pm i\pi/3)$, respectively.

shiftUC. Equation (6) takes the following form:

$$(\mathbf{c}_1, \mathbf{c}_2, \mathbf{c}_3)^T = \begin{pmatrix} 1 & -1 & 0 \\ 0 & 1 & -1 \\ 1 & 1 & 1 \end{pmatrix} (\mathbf{a}_1, \mathbf{a}_2, \mathbf{a}_3)^T, \quad (13)$$

so **refUC** = 1, -1, 0, 0, 1, -1, 1, 1, 1. In the following lines, which have been taken from the output of **IrRep** available among the examples in **IrRep**'s Github repository[68], we show how **IrRep** prints the matrix of symmetry operations, in particular for the 3-fold rotation, in the settings before and after applying the transformation of the unit cell:

```

1 # 3
2 rotation : | 0 0 1 |      in refUC : | 0 -1 0 |
3           | 1 0 0 |           | 1 -1 0 |
4           | 0 1 0 |           | 0 0 1 |
5 spinor    : | 0.500-0.866j -0.000-0.000j |
6           | 0.000-0.000j  0.500+0.866j |
7 translation : [ 0.000000 0.000000 0.000000 ]
8           in the reference unit cell :
9           translation : [ 0.000000 0.000000 0.000000 ]
10 axis: [0. 0. 1.] ; angle = 2/3 pi, inversion : False

```

To make sure that the transformation is correct, one has to check whether matrices and translation vectors after the change of basis match with those in the table file of the corresponding space group. Alternatively, they can be compared to matrices and translations in the GENPOS application of the BCS[72]. The next step is to calculate the IRs of occupied bands (Tab. 4). For that, we call **IrRep** with the keywords written in the following lines:

```

1 python -m spinor=T code=vasp kpname=T,GM,F,L Ecut=50 refUC
    =1,-1,0,0,1,-1,1,1,1 EF=5.2156 IBstart=5 IBend=10

```

T	Γ	F	L
$\bar{T}_9 \oplus \bar{T}_8 \oplus \bar{T}_6 \bar{T}_7$	$2\bar{\Gamma}_8 \oplus \bar{\Gamma}_4 \bar{\Gamma}_5$	$\bar{F}_3 \bar{F}_4 \oplus \bar{F}_5 \bar{F}_6 \oplus \bar{F}_5 \bar{F}_6$	$\bar{L}_5 \bar{L}_6 \oplus \bar{L}_3 \bar{L}_4 \oplus \bar{L}_5 \bar{L}_6$

Table 4: IRs at TRIM for the last 6 occupied bands in Bi, calculated with **IrRep**. In each k -point, IRs are written from left to right in ascending energy order, e.g., $\bar{T}_6 \bar{T}_7$ is higher in energy than \bar{T}_8 .

With the knowledge of the IRs and their inversion eigenvalues [see Fig. 5(a)], we conclude that the total number of (Kramers pairs of) -1 inversion eigenvalues in the occupied bands is even, thus the \mathbb{Z}_2 index $z_2 = +1$. However, there are two band inversions between Γ and T that the \mathbb{Z}_2 invariant cannot detect. Indeed, this double band-inversion leads to the \mathbb{Z}_4 invariant $z_4 = 2$, since the number of Kramers pairs of -1 inversion eigenvalues is equal to 2 mod 4. This means that Bi is a higher-order topological insulator (HOTI) [27]. The value of the \mathbb{Z}_4 index and number of -1 inversion eigenvalues are, by default, calculated and printed by **IrRep**; in the following line, we show the way in which they are printed by the code, together with information about the direct and general gaps:¹

```

1 Number of inversions-odd Kramers pairs IN THE LISTED KPOINTS: 6      Z4= 2
2 Minimal direct gap: 0.08857033154551353 eV
3 Indirect gap: -0.1886089499035215 eV

```

5. Conclusion

IrRep is a Python code for the calculation of irreducible representations of DFT calculated bands at high-symmetry points. It is a powerful tool for the detection and classification of topological sets of bands and materials, applicable with calculations performed both with or without SOC and using unit cells that might be non-conventional. Its structure keeps the implementation of interfaces to plane-wave DFT codes simple; currently, it is compatible with VASP, Abinit, Quantum Espresso and any code that has an interface to Wannier90 (which covers most of the popular DFT codes). Additionally, routines for separating bands based on an eigenvalue of certain symmetry operation are included. **IrRep** can be freely downloaded from <https://github.com/stepan-tsirkin/irrep> and/or installed with **pip**; the repository also contains examples, including the analysis of CuBi_2O_4 that we have presented in this work to illustrate the utility of the code.

Software availability

All software used and developed in this article (except VASP) is open-source and available for free. **IrRep** is available via **pip** [73] and GitHub [68]. External libraries used in **IrRep** include **spglib** [56], **NumPy** [74], **SciPy** [75], and **lazy-property** [76]. VASP is commercial software available from the developers for a fee [77]. Other codes are available at

¹here the gap refers only to the high-symmetry points included in the calculation. The real gap may be smaller (and even may close) at some arbitrary point away from high-symmetry points.

[78] (Wannier90), [79] (QuantumEspresso) and [80] (Abinit). Figures of crystal structures were generated with VESTA [81]. Band structures were plotted with BEplot [82], which uses Matplotlib [83]. Inkscape vector graphics editor [84] was used in most figures.

Acknowledgements

M.G.V. and M.I. acknowledges the Spanish Ministerio de Ciencia e Innovacion (grant number PID2019-109905GB-C21) and DFG INCIEN2019-000356 from Gipuzkoako Foru Al-
 undia. B. B. acknowledges the support of the Alfred P. Sloan foundation, and the National Science Foundation under grant DMR-1945058. The work of J.L.M. has been supported by Spanish Science Ministry grant PGC2018-094626-BC21 (MCIU/AEI/FEDER, EU) and Basque Government grant IT979-16. S.S.T. and T.N. acknowledge support from NCRR Marvel and from the European Unions Horizon 2020 research and innovation program (ERC-StG-Neupert-757867-PARATOP). S.S.T. also acknowledges support from the Swiss National Science Foundation (grant number: PP00P2_176877).

References

- [1] H. Weyl, The theory of groups and quantum mechanics, Courier Corporation, 1950.
- [2] L. P. Bouckaert, R. Smoluchowski, E. Wigner, Theory of brillouin zones and symmetry properties of wave functions in crystals, Physical Review 50 (1) (1936) 58.
- [3] C. Bradley, A. Cracknell, The Mathematical Theory of Symmetry in Solids: Representation Theory for Point Groups and Space Groups, Clarendon Press, Oxford, 2010.
- [4] C. L. Kane, E. J. Mele, Quantum spin Hall effect in graphene, Phys. Rev. Lett. 95 (2005) 226801. doi:10.1103/PhysRevLett.95.226801.
 URL <https://link.aps.org/doi/10.1103/PhysRevLett.95.226801>
- [5] B. A. Bernevig, S.-C. Zhang, Quantum spin Hall effect, Phys. Rev. Lett. 96 (2006) 106802. doi:10.1103/PhysRevLett.96.106802.
 URL <https://link.aps.org/doi/10.1103/PhysRevLett.96.106802>
- [6] L. Fu, C. L. Kane, Topological insulators with inversion symmetry, Phys. Rev. B 76 (2007) 045302. doi:10.1103/PhysRevB.76.045302.
 URL <https://link.aps.org/doi/10.1103/PhysRevB.76.045302>
- [7] J. C. Y. Teo, L. Fu, C. L. Kane, Surface states and topological invariants in three-dimensional topological insulators: Application to $\text{Bi}_{1-x}\text{Sb}_x$, Phys. Rev. B 78 (2008) 045426. doi:10.1103/PhysRevB.78.045426.
 URL <https://link.aps.org/doi/10.1103/PhysRevB.78.045426>
- [8] A. M. Turner, Y. Zhang, A. Vishwanath, Entanglement and inversion symmetry in topological insulators, Phys. Rev. B 82 (2010) 241102. doi:10.1103/PhysRevB.82.241102.
 URL <https://link.aps.org/doi/10.1103/PhysRevB.82.241102>

- [9] T. L. Hughes, E. Prodan, B. A. Bernevig, Inversion-symmetric topological insulators, *Phys. Rev. B* 83 (2011) 245132. doi:10.1103/PhysRevB.83.245132.
URL <https://link.aps.org/doi/10.1103/PhysRevB.83.245132>
- [10] L. Fu, Topological crystalline insulators, *Phys. Rev. Lett.* 106 (2011) 106802. doi:10.1103/PhysRevLett.106.106802.
URL <https://link.aps.org/doi/10.1103/PhysRevLett.106.106802>
- [11] T. H. Hsieh, H. Lin, J. Liu, W. Duan, A. Bansil, L. Fu, Topological crystalline insulators in the SnTe material class, *Nature Communications* 3 (2012) 932.
- [12] A. M. Turner, Y. Zhang, R. S. K. Mong, A. Vishwanath, Quantized response and topology of magnetic insulators with inversion symmetry, *Phys. Rev. B* 85 (2012) 165120. doi:10.1103/PhysRevB.85.165120.
URL <https://link.aps.org/doi/10.1103/PhysRevB.85.165120>
- [13] B. Bradlyn, L. Elcoro, J. Cano, M. G. Vergniory, Z. Wang, C. Felser, M. I. Aroyo, B. A. Bernevig, Topological quantum chemistry, *Nature* 547 (7663) (2017) 298–305. doi:10.1038/nature23268.
URL <https://doi.org/10.1038/nature23268>
- [14] B. Bradlyn, L. Elcoro, M. G. Vergniory, J. Cano, Z. Wang, C. Felser, M. I. Aroyo, B. A. Bernevig, Band connectivity for topological quantum chemistry: Band structures as a graph theory problem, *Phys. Rev. B* 97 (2018) 035138. doi:10.1103/PhysRevB.97.035138.
URL <https://link.aps.org/doi/10.1103/PhysRevB.97.035138>
- [15] M. G. Vergniory, L. Elcoro, Z. Wang, J. Cano, C. Felser, M. I. Aroyo, B. A. Bernevig, B. Bradlyn, Graph theory data for topological quantum chemistry, *Phys. Rev. E* 96 (2017) 023310. doi:10.1103/PhysRevE.96.023310.
URL <https://link.aps.org/doi/10.1103/PhysRevE.96.023310>
- [16] J. Cano, B. Bradlyn, Band representations and topological quantum chemistry, arXiv preprint arXiv:2006.04890 (2020).
- [17] H. C. Po, Symmetry indicators of band topology, *Journal of Physics: Condensed Matter* 32 (26) (2020) 263001.
- [18] L. Elcoro, Z. Song, B. A. Bernevig, Application of the induction procedure and the Smith decomposition in the calculation and topological classification of electronic band structures in the 230 space groups, arXiv preprint arXiv:2002.03836 (2020).
- [19] Z. Song, T. Zhang, Z. Fang, C. Fang, Quantitative mappings between symmetry and topology in solids, *Nature Communications* 9 (1) (2018) 3530. doi:10.1038/s41467-018-06010-w.
URL <https://doi.org/10.1038/s41467-018-06010-w>

- [20] H. C. Po, A. Vishwanath, H. Watanabe, Symmetry-based indicators of band topology in the 230 space groups, *Nature Communications* 8 (1) (2017) 50. doi:10.1038/s41467-017-00133-2.
URL <https://doi.org/10.1038/s41467-017-00133-2>
- [21] M. G. Vergniory, L. Elcoro, C. Felser, N. Regnault, B. A. Bernevig, Z. Wang, A complete catalogue of high-quality topological materials, *Nature* 566 (7745) (2019) 480–485. doi:10.1038/s41586-019-0954-4.
URL <https://doi.org/10.1038/s41586-019-0954-4>
- [22] T. Zhang, Y. Jiang, Z. Song, H. Huang, Y. He, Z. Fang, H. Weng, C. Fang, Catalogue of topological electronic materials, *Nature* 566 (7745) (2019) 475–479. doi:10.1038/s41586-019-0944-6.
URL <https://doi.org/10.1038/s41586-019-0944-6>
- [23] F. Tang, H. C. Po, A. Vishwanath, X. Wan, Efficient topological materials discovery using symmetry indicators, *Nature Physics* 15 (5) (2019) 470–476. doi:10.1038/s41567-019-0418-7.
URL <https://doi.org/10.1038/s41567-019-0418-7>
- [24] Y. Xu, L. Elcoro, Z. Song, B. J. Wieder, M. Vergniory, N. Regnault, Y. Chen, C. Felser, B. A. Bernevig, G. Sharma, et al., High-throughput calculations of antiferromagnetic topological materials from magnetic topological quantum chemistry, *arXiv preprint arXiv:2003.00012* (2020).
- [25] H. C. Po, H. Watanabe, A. Vishwanath, Fragile topology and Wannier obstructions, *arXiv preprint arXiv:1709.06551* (2017).
URL <https://arxiv.org/abs/1709.06551>
- [26] F. Schindler, A. M. Cook, M. G. Vergniory, Z. Wang, S. S. P. Parkin, B. A. Bernevig, T. Neupert, Higher-order topological insulators, *Science Advances* 4 (6) (2018). arXiv:<https://advances.sciencemag.org/content/4/6/eaat0346.full.pdf>, doi:10.1126/sciadv.aat0346.
URL <https://advances.sciencemag.org/content/4/6/eaat0346>
- [27] F. Schindler, Z. Wang, M. G. Vergniory, A. M. Cook, A. Murani, S. Sengupta, A. Y. Kasumov, R. Deblock, S. Jeon, I. Drozdov, H. Bouchiat, S. Guéron, A. Yazdani, B. A. Bernevig, T. Neupert, Higher-order topology in bismuth, *Nature Physics* 14 (2018) 918. doi:10.1038/s41567-018-0224-7.
URL <https://doi.org/10.1038/s41567-018-0224-7>
- [28] F. Schindler, M. Brzezińska, W. A. Benalcazar, M. Iraola, A. Bouhon, S. S. Tsirkin, M. G. Vergniory, T. Neupert, Fractional corner charges in spin-orbit coupled crystals, *Phys. Rev. Research* 1 (2019) 033074. doi:10.1103/PhysRevResearch.1.033074.
URL <https://link.aps.org/doi/10.1103/PhysRevResearch.1.033074>

- [29] M. B. de Paz, M. G. Vergniory, D. Bercioux, A. García-Etxarri, B. Bradlyn, Engineering fragile topology in photonic crystals: Topological quantum chemistry of light, *Phys. Rev. Research* 1 (2019) 032005. doi:10.1103/PhysRevResearch.1.032005. URL <https://link.aps.org/doi/10.1103/PhysRevResearch.1.032005>
- [30] B. Bradlyn, Z. Wang, J. Cano, B. A. Bernevig, Disconnected elementary band representations, fragile topology, and Wilson loops as topological indices: An example on the triangular lattice, *Phys. Rev. B* 99 (2019) 045140. doi:10.1103/PhysRevB.99.045140. URL <https://link.aps.org/doi/10.1103/PhysRevB.99.045140>
- [31] B. J. Wieder, B. A. Bernevig, The axion insulator as a pump of fragile topology, *arXiv preprint arXiv:1810.02373* (2018). URL <https://arxiv.org/abs/1810.02373>
- [32] B. J. Wieder, Z. Wang, J. Cano, X. Dai, L. M. Schoop, B. Bradlyn, B. A. Bernevig, Strong and fragile topological Dirac semimetals with higher-order Fermi arcs, *Nature communications* 11 (1) (2020) 1–13.
- [33] W. Shi, B. J. Wieder, H. Meyerheim, Y. Sun, Y. Zhang, Y. Li, L. Shen, Y. Qi, L. Yang, J. Jena, et al., A charge-density-wave Weyl semimetal, *arXiv preprint arXiv:1909.04037* (2019).
- [34] J. Gooth, B. Bradlyn, S. Honnali, C. Schindler, N. Kumar, J. Noky, Y. Qi, C. Shekhar, Y. Sun, Z. Wang, B. A. Bernevig, C. Felser, Axionic charge-density wave in the Weyl semimetal $(\text{TaSe}_4)_2\text{I}$, *Nature* 575 (7782) (2019) 315–319. doi:10.1038/s41586-019-1630-4. URL <https://doi.org/10.1038/s41586-019-1630-4>
- [35] Z. Wang, B. J. Wieder, J. Li, B. Yan, B. A. Bernevig, Higher-order topology, monopole nodal lines, and the origin of large Fermi arcs in transition metal dichalcogenides XTe_2 ($\text{X} = \text{Mo}, \text{W}$), *Physical review letters* 123 (18) (2019) 186401.
- [36] G. Kresse, J. Furthmüller, Efficient iterative schemes for ab initio total-energy calculations using a plane-wave basis set, *Phys. Rev. B* 54 (1996) 11169–11186. doi:10.1103/PhysRevB.54.11169. URL <https://link.aps.org/doi/10.1103/PhysRevB.54.11169>
- [37] X. Gonze, F. Jollet, F. Abreu Araujo, D. Adams, B. Amadon, T. Applencourt, C. Audouze, J.-M. Beuken, J. Bieder, A. Bokhanchuk, E. Bousquet, F. Bruneval, D. Caliste, M. Ct, F. Dahm, F. Da Pieve, M. Delaveau, M. Di Gennaro, B. Dorado, C. Espejo, G. Geneste, L. Genovese, A. Gerossier, M. Giantomassi, Y. Gillet, D. Hamann, L. He, G. Jomard, J. Laflamme Janssen, S. Le Roux, A. Levitt, A. Lherbier, F. Liu, I. Lukaevi, A. Martin, C. Martins, M. Oliveira, S. Ponc, Y. Pouillon, T. Rangel, G.-M. Rignanese, A. Romero, B. Rousseau, O. Rubel, A. Shukri, M. Stankovski, M. Torrent, M. Van Setten, B. Van Troeye, M. Verstraete, D. Waroquiers, J. Wiktor, B. Xu, A. Zhou, J. Zwanziger, Recent developments in the ABINIT software package, *Comput.*

- Phys. Commun. 205 (2016) 106–131. doi:10.1016/j.cpc.2016.04.003.
URL <https://doi.org/10.1016/j.cpc.2016.04.003>
- [38] P. Giannozzi, S. Baroni, N. Bonini, M. Calandra, R. Car, C. Cavazzoni, D. Ceresoli, G. L. Chiarotti, M. Cococcioni, I. Dabo, A. D. Corso, S. de Gironcoli, S. Fabris, G. Fratesi, R. Gebauer, U. Gerstmann, C. Gougoussis, A. Kokalj, M. Lazzeri, L. Martin-Samos, N. Marzari, F. Mauri, R. Mazzarello, S. Paolini, A. Pasquarello, L. Paulatto, C. Sbraccia, S. Scandolo, G. Sclauzero, A. P. Seitsonen, A. Smogunov, P. Umari, R. M. Wentzcovitch, QUANTUM ESPRESSO: a modular and open-source software project for quantum simulations of materials, *Journal of Physics: Condensed Matter* 21 (39) (2009) 395502. doi:10.1088/0953-8984/21/39/395502.
URL <https://doi.org/10.1088/0953-8984/21/39/395502>
- [39] G. Pizzi, V. Vitale, R. Arita, S. Blgel, F. Freimuth, G. Géranton, M. Gibertini, D. Gresch, C. Johnson, T. Koretsune, J. Ibañez-Azpiroz, H. Lee, J.-M. Lihm, D. Marchand, A. Marrazzo, Y. Mokrousov, J. I. Mustafa, Y. Nohara, Y. Nomura, L. Paulatto, S. Poncé, T. Ponweiser, J. Qiao, F. Thle, S. S. Tsirkin, M. Wierzbowska, N. Marzari, D. Vanderbilt, I. Souza, A. A. Mostofi, J. R. Yates, Wannier90 as a community code: new features and applications, *Journal of Physics: Condensed Matter* 32 (16) (2020) 165902. doi:10.1088/1361-648x/ab51ff.
URL <https://doi.org/10.1088/1361-648x/ab51ff>
- [40] J. M. Soler, E. Artacho, J. D. Gale, A. García, J. Junquera, P. Ordejón, D. Sánchez-Portal, The SIESTA method for *ab initio* order-*n* materials simulation, *Journal of Physics: Condensed Matter* 14 (11) (2002) 2745–2779. doi:10.1088/0953-8984/14/11/302.
URL <https://doi.org/10.1088/0953-8984/14/11/302>
- [41] J. Gao, Q. Wu, C. Persson, Z. Wang, Irvsp: to obtain irreducible representations of electronic states in the VASP (2020). arXiv:2002.04032.
- [42] Topological materials database, <https://topologicalquantumchemistry.org> (2019).
- [43] A. Matsugatani, S. Ono, Y. Nomura, H. Watanabe, qeirreps: an open-source program for quantum espresso to compute irreducible representations of bloch wavefunctions, arXiv preprint arXiv:2006.00194 (2020).
- [44] Bilbao Crystallographic Server, <https://www.cryst.ehu.es/>.
- [45] S. S. Tsirkin, I. Souza, D. Vanderbilt, Composite Weyl nodes stabilized by screw symmetry with and without time-reversal invariance, *Phys. Rev. B* 96 (2017) 045102. doi:10.1103/PhysRevB.96.045102.
URL <https://link.aps.org/doi/10.1103/PhysRevB.96.045102>
- [46] J. F. Khoury, A. J. E. Rettie, M. A. Khan, N. J. Ghimire, I. n. Robredo, J. E. Pfluger, K. Pal, C. Wolverton, A. Bergara, J. S. Jiang, L. M. Schoop, M. G. Vergniory,

- J. F. Mitchell, D. Y. Chung, M. G. Kanatzidis, A new three-dimensional subsulfide $\text{Ir}_2\text{In}_8\text{S}$ with Dirac semimetal behavior, *Journal of the American Chemical Society* 141 (48) (2019) 19130–19137, pMID: 31697089. arXiv:<https://doi.org/10.1021/jacs.9b10147>, doi:10.1021/jacs.9b10147.
URL <https://doi.org/10.1021/jacs.9b10147>
- [47] J. F. Khoury, A. J. E. Rettie, I. n. Robredo, M. J. Krogstad, C. D. Malliakas, A. Bergara, M. G. Vergniory, R. Osborn, S. Rosenkranz, D. Y. Chung, M. G. Kanatzidis, The subchalcogenides $\text{Ir}_2\text{In}_8\text{Q}$ ($\text{Q} = \text{S}, \text{Se}, \text{Te}$): Dirac semimetal candidates with re-entrant structural modulation, *Journal of the American Chemical Society* 142 (13) (2020) 6312–6323, pMID: 32160464. arXiv:<https://doi.org/10.1021/jacs.0c00809>, doi:10.1021/jacs.0c00809.
URL <https://doi.org/10.1021/jacs.0c00809>
- [48] I. Robredo, M. G. Vergniory, B. Bradlyn, Higher-order and crystalline topology in a phenomenological tight-binding model of lead telluride, *Phys. Rev. Materials* 3 (2019) 041202. doi:10.1103/PhysRevMaterials.3.041202.
URL <https://link.aps.org/doi/10.1103/PhysRevMaterials.3.041202>
- [49] M.-Á. Sánchez-Martínez, I. Robredo, A. Bidaurreazaga, A. Bergara, F. de Juan, A. G. Grushin, M. G. Vergniory, Spectral and optical properties of $\text{Ag}_3\text{Au}(\text{Se}_2, \text{Te}_2)$ and dark matter detection, *Journal of Physics: Materials* 3 (1) (2019) 014001. doi:10.1088/2515-7639/ab3ea2.
URL <https://doi.org/10.1088%2F2515-7639%2Fab3ea2>
- [50] J. Ibañez-Azpiroz, F. de Juan, I. Souza, Quantitative analysis of two-band $k \cdot p$ models describing the shift-current photoconductivity (2019). arXiv:1910.06172.
- [51] J. Ibañez Azpiroz, I. Souza, F. de Juan, Directional shift current in mirror-symmetric bc_2N , *Phys. Rev. Research* 2 (2020) 013263. doi:10.1103/PhysRevResearch.2.013263.
URL <https://link.aps.org/doi/10.1103/PhysRevResearch.2.013263>
- [52] <https://pepy.tech/project/irrep>.
- [53] M. I. Aroyo (Ed.), *International Tables for Crystallography*, Vol. A, International Union of Crystallography, 2016. doi:10.1107/97809553602060000114.
URL <http://it.iucr.org/A/>
- [54] L. Elcoro, B. Bradlyn, Z. Wang, M. G. Vergniory, J. Cano, C. Felser, B. A. Bernevig, D. Orobengoa, G. de la Flor, M. I. Aroyo, Double crystallographic groups and their representations on the Bilbao Crystallographic Server, *Journal of Applied Crystallography* 50 (5) (2017) 1457–1477. doi:10.1107/S1600576717011712.
URL <https://doi.org/10.1107/S1600576717011712>
- [55] J. P. Serre, *Linear Representations of Finite Groups*, Springer, 1996.

- [56] A. Togo, I. Tanaka, Spglib: a software library for crystal symmetry search (2018). [arXiv:1808.01590](https://arxiv.org/abs/1808.01590).
- [57] P. E. Blöchl, Projector augmented-wave method, *Phys. Rev. B* 50 (1994) 17953–17979. doi:10.1103/PhysRevB.50.17953. URL <https://link.aps.org/doi/10.1103/PhysRevB.50.17953>
- [58] G. Kresse, D. Joubert, From ultrasoft pseudopotentials to the projector augmented-wave method, *Phys. Rev. B* 59 (1999) 1758–1775. doi:10.1103/PhysRevB.59.1758. URL <https://link.aps.org/doi/10.1103/PhysRevB.59.1758>
- [59] M. Torrent, F. Jollet, F. Bottin, G. Zrah, X. Gonze, Implementation of the projector augmented-wave method in the ABINIT code: Application to the study of iron under pressure, *Computational Materials Science* 42 (2) (2008) 337–351. doi:10.1016/j.commatsci.2007.07.020. URL <https://doi.org/10.1016/j.commatsci.2007.07.020>
- [60] J. E. Moore, L. Balents, Topological invariants of time-reversal-invariant band structures, *Phys. Rev. B* 75 (2007) 121306. doi:10.1103/PhysRevB.75.121306. URL <https://link.aps.org/doi/10.1103/PhysRevB.75.121306>
- [61] K. Yamada, K.-i. Takada, S. Hosoya, Y. Watanabe, Y. Endoh, N. Tomonaga, T. Suzuki, T. Ishigaki, T. Kamiyama, H. Asano, F. Izumi, Three-dimensional antiferromagnetic order and anisotropic magnetic properties in Bi_2CuO_4 , *Journal of the Physical Society of Japan* 60 (7) (1991) 2406–2414. [arXiv:https://doi.org/10.1143/JPSJ.60.2406](https://arxiv.org/abs/https://doi.org/10.1143/JPSJ.60.2406), doi:10.1143/JPSJ.60.2406. URL <https://doi.org/10.1143/JPSJ.60.2406>
- [62] D. Thomas, J.-C. Boivin, J. Trhoux, tude structurale de CuBi_2O_4 , *Bulletin de la Socit franaise de Minralogie et de Cristallographie* 99 (4) (1976) 193–196. doi:10.3406/bulmi.1976.7065. URL https://www.persee.fr/doc/bulmi_0037-9328_1976_num_99_4_7065
- [63] B. Bradlyn, J. Cano, Z. Wang, M. G. Vergniory, C. Felser, R. J. Cava, B. A. Bernevig, Beyond Dirac and Weyl fermions: Unconventional quasiparticles in conventional crystals, *Science* 353 (6299) (2016). [arXiv:https://science.sciencemag.org/content/353/6299/aaf5037.full.pdf](https://arxiv.org/abs/https://science.sciencemag.org/content/353/6299/aaf5037.full.pdf), doi:10.1126/science.aaf5037. URL <https://science.sciencemag.org/content/353/6299/aaf5037>
- [64] B. J. Wieder, Y. Kim, A. Rappe, C. Kane, Double Dirac semimetals in three dimensions, *Physical review letters* 116 (18) (2016) 186402.
- [65] N. Marzari, Ab-initio Molecular Dynamics for Metallic Systems. PhD Thesis, http://theosrv1.epfl.ch/Main/Theses?action=download&upname=Marzari_thesis_1996.pdf (1996).

- [66] J. P. Perdew, K. Burke, M. Ernzerhof, Generalized gradient approximation made simple, Phys. Rev. Lett. 77 (1996) 3865–3868. doi:10.1103/PhysRevLett.77.3865.
URL <https://link.aps.org/doi/10.1103/PhysRevLett.77.3865>
- [67] [database] Pseudo Dojo database of pseudopotentials, <http://www.pseudo-dojo.org/index.html>.
- [68] Official repository of Irrep, <https://github.com/stepan-tsirkin/irrep>.
- [69] J. Zak, Symmetry specification of bands in solids, Phys. Rev. Lett. 45 (1980) 1025–1028. doi:10.1103/PhysRevLett.45.1025.
URL <https://link.aps.org/doi/10.1103/PhysRevLett.45.1025>
- [70] J. Zak, Band representations and symmetry types of bands in solids, Phys. Rev. B 23 (1981) 2824–2835. doi:10.1103/PhysRevB.23.2824.
URL <https://link.aps.org/doi/10.1103/PhysRevB.23.2824>
- [71] C. L. Kane, E. J. Mele, z_2 topological order and the quantum spin Hall effect, Physical review letters 95 (14) (2005) 146802.
- [72] M. I. Aroyo, J. M. Perez-Mato, C. Capillas, E. Kroumova, S. Ivantchev, G. Madariaga, A. Kirov, H. Wondratschek, Bilbao Crystallographic Server: I. Databases and crystallographic computing programs, Zeitschrift für Kristallographie - Crystalline Materials 221 (1) (2006) 15 – 27. doi:<https://doi.org/10.1524/zkri.2006.221.1.15>.
URL <https://www.degruyter.com/view/journals/zkri/221/1/article-p15.xml>
- [73] PyPI repository, <https://pypi.org/project/irrep>.
- [74] T. E. Oliphant, A guide to NumPy, Vol. 1, Trelgol Publishing USA, 2006.
- [75] P. Virtanen, R. Gommers, T. E. Oliphant, M. Haberland, T. Reddy, D. Cournapeau, E. Burovski, P. Peterson, W. Weckesser, J. Bright, S. J. van der Walt, M. Brett, J. Wilson, K. Jarrod Millman, N. Mayorov, A. R. J. Nelson, E. Jones, R. Kern, E. Larson, C. Carey, Í. Polat, Y. Feng, E. W. Moore, J. Vand erPlas, D. Laxalde, J. Perktold, R. Cimrman, I. Henriksen, E. A. Quintero, C. R. Harris, A. M. Archibald, A. H. Ribeiro, F. Pedregosa, P. van Mulbregt, S. . . Contributors, SciPy 1.0: Fundamental Algorithms for Scientific Computing in Python, Nature Methods (2020). doi:<https://doi.org/10.1038/s41592-019-0686-2>.
- [76] lazy-property python module, <https://pypi.org/project/lazy-property>.
- [77] VASP code, <https://www.vasp.at/>.
- [78] Wannier90 code, <http://www.wannier.org/>.
- [79] QuantumEspresso code, <https://www.quantum-espresso.org/>.
- [80] Abinit code, <https://www.abinit.org/>.

- [81] K. Momma, F. Izumi, *VESTA3* for three-dimensional visualization of crystal, volumetric and morphology data, *Journal of Applied Crystallography* 44 (6) (2011) 1272–1276. doi:10.1107/S0021889811038970.
URL <https://doi.org/10.1107/S0021889811038970>
- [82] Repository of BEplot, <https://gitlab.com/Miraola/BEplot>.
- [83] J. D. Hunter, Matplotlib: A 2D graphics environment, *Computing in Science & Engineering* 9 (3) (2007) 90–95. doi:10.1109/MCSE.2007.55.
- [84] Inkscape vector graphics editor, <https://inkscape.org>.